Acta Crystallographica Section D
Biological Crystallography
ISSN 0907-4449

Structure of *Mycobacterium tuberculosis* chaperonin-10 at 3.5 Å resolution

Bhupesh Taneja and Shekhar C. Mande

Acta Crystallographica Section D
Biological Crystallography
ISSN 0907-4449

Structure of *Mycobacterium tuberculosis* chaperonin-10 at 3.5 Å resolution

Bhupesh Taneja and Shekhar C. Mande*†

Institute of Microbial Technology, Sector 39-A, Chandigarh 160 036, India

† Address for correspondence: Centre for DNA Fingerprinting and Diagnostics, ECIL Road, Nacharam, Hyderabad 500 076, India.

Correspondence e-mail: shekhar@www.cdfd.org.in

Received 30 July 2001
Accepted 7 November 2001

PDB Reference: chaperonin-10, 1hx5.

Chaperonin-60 (cpn60) and chaperonin-10 (cpn10) are essential proteins involved in ATP-dependent folding of several intracellular proteins in the bacterial cell. Folding of the nascent substrate polypeptide takes place in the large central cavity formed by each ring of the tetradecameric cpn60. This large cavity is closed upon capping by the heptameric cpn10. Cpn10s interact with cpn60s primarily through a 17-residue mobile loop and regulate the release and binding of the substrate polypeptide from the cpn60 surface. Here, the structure of *M. tuberculosis* cpn10 is reported at 3.5 Å resolution. The overall structure of the cpn10 monomer is formed of a four-stranded β-barrel and two long stretches of highly flexible segments: the dome loop and the mobile loop. The seven subunits in the heptamer show very little conformational difference and exhibit nearly perfect seven-fold geometry. The binding sites for metal ions in the dome loop of cpn10 have been identified, suggesting the role of metal ions in the stabilization of the protein. Comparisons with the available cpn10 structures indicate several interesting features.

1. Introduction

Chaperonin-60 (cpn60) and chaperonin-10 (cpn10) have served as a paradigm for chaperone-mediated protein folding, with numerous elegant experiments resulting in a very fascinating and intricate mechanism for the protein-folding reaction (Hartl, 1996; Fenton & Horwich, 1997; Sigler *et al.*, 1998). Ubiquitously present, the chaperonins are known to be essential components of cells at all temperatures (Fayet *et al.*, 1989) and assist the folding of a variety of proteins in *Escherichia coli* (Houry *et al.*, 1999). Despite this, many aspects of the chaperonin-mediated protein-folding reaction remain unknown.

Cpn60 is a homo-tetradecamer of 60 kDa subunits organized into two heptameric rings arranged back to back (Sigler *et al.*, 1998). Protein-folding processes *in vivo* occur in the large cavity of the tetradecameric cpn60 cylinder, where unfolded or partially folded polypeptides are sequestered. Release and binding of polypeptides from the cpn60 surface is tightly regulated by cpn10. Cpn10 and its homologues from other species form a loose heptameric assembly of identical 10 kDa subunits (Hunt *et al.*, 1996, 1997; Mande *et al.*, 1996). Binding of ATP and a cpn10 heptamer to the *cis* ring of the cpn60 tetradecamer results in an enlarged hydrophilic central cavity that sequesters the polypeptides from external factors and provides a suitable environment for them to fold (Hartl, 1996; Fenton & Horwich, 1997; Xu *et al.*, 1997). ATP hydrolysis in the *cis* ring accompanied by ATP binding in the *trans*

Table 1
Data reduction and final refinement statistics of Mt-cpn10.

Values in parentheses are for the highest resolution shell (3.77–3.5 Å).

Crystallographic data	
Space group	$C222_1$
Unit-cell parameters	
a (Å)	77.5
b (Å)	162.5
c (Å)	125.6
Resolution range (Å)	30–3.5
Completeness of data (%)	96.4 (90.5)
$R_{\rm merge}$ (%)	7.8 (28.0)
$I/\sigma(I)$ (overall)	11.7
Matthews number ($V_{\rm M}$) (Å^3 Da^{-1})	2.8
Solvent content in the crystal (%)	45
Refinement data	
Total No. of reflections	9927
No. of reflections for $R_{\rm free}$ calculations	478
$R/R_{\rm free}$ (%)	20.2/26.5
Ramachandran plot statistics	
Residues in most allowed regions (heptamer) (%)	89.1
Residues in disallowed regions (heptamer) (%)	0.9
Overall G factor	−0.14
$R_{\rm merge}$ of mercury-derived crystal to its maximum resolution of 6.0 Å (%)	8.4
$R_{\rm deriv}$ (mercury-derived data merged with native data) (%)	19.1

ring promotes cpn10 dissociation from the complex and allows the substrate polypeptide to diffuse from the central cavity of cpn60 (Rye *et al.*, 1997).

Large conformational changes are known to take place in the uncomplexed and complexed forms of cpn60 (Xu *et al.*, 1997). The conformational changes involve an outward movement of the apical domain in cpn60, resulting in almost a doubling of the cavity volume underneath the cpn10 heptamer. Similarly, cpn10 also undergoes major structural rearrangements before associating with cpn60. The conformational changes that take place in cpn10 on association with cpn60 involve the loss in flexibility of an approximately 17-residue stretch commonly referred to as the 'mobile loop'. Elegant NMR studies have shown that the mobile loop is highly flexible in isolated cpn10 but becomes rigid on association with cpn60 (Landry *et al.*, 1993). We have recently solved the crystal structure of the *M. tuberculosis* cpn10 (Mt-cpn10) encoded by the Rv3418c ORF of the *M. tuberculosis* genome (Cole *et al.*, 1998) and identified a partially stable conformation of its mobile loop (Taneja & Mande, 2001*b*). We have now identified the binding site for metal ions in the dome loop of Mt-cpn10 which have previously been shown to modulate the different plastic states of Mt-cpn10 (Fossati *et al.*, 1995; Taneja & Mande, 2001*a*).

Bacterial chaperonins of certain species, including those derived from mycobacteria, are highly antigenic. On the other hand, the *E. coli* and human cpn10s do not elicit a strong immune response (Richardson *et al.*, 2001). Previous studies have identified the strongly immunodominant epitopes from *M. leprae* cpn10 (Kim *et al.*, 1997). Similarly, immunodominant regions of the *M. tuberculosis* cpn10 have also been identified (Chua-Intra *et al.*, 1998). Species-specific immunodominant epitopes of the mycobacterial chaperonins have been mapped earlier onto certain regions of the mobile loop (Mande *et al.*, 1996; Kim *et al.*, 1997). With the availability of crystal structures of both these antigens, we can now begin to address questions relating to their interesting immunological properties.

2. Materials and methods

2.1. Crystallization and data collection

The highly plastic nature of Mt-cpn10 caused major difficulties in obtaining suitable diffraction-quality crystals. Mt-cpn10 cloned in the pMAL-c vector, a kind gift from Drs Vijay Mehra and Barry Bloom, contained seven additional residues at the N-terminal arising from the choice of restriction sites during cloning (Mehra *et al.*, 1992). These seven residues were likely to be mobile in solution and it was possible that they interfered in the crystallization process. Consequently, although crystals could be grown to sizes as large as 0.5 × 0.5 × 0.5 mm, none of these led to diffraction beyond 8 Å resolution. As a first step towards obtaining good crystals, therefore, we removed the seven additional residues by site-directed mutagenesis (Taneja & Mande, 2001*a*). This protein could be purified in large amounts for further experimentation.

The protein was then screened for crystallization in complex with divalent cations using the hanging-drop vapour-diffusion method. Several different conditions were screened with the addition of a variety of divalent cations to obtain suitable crystals. Finally, suitable crystals were obtained with 14 mg ml^{-1} protein in the presence of 10 m*M* $CaCl_2$ using a well solution consisting of 26% PEG 400, 210 m*M* Li_2SO_4, 100 m*M* sodium acetate buffer pH 4.0, as previously described by Taneja & Mande (2001*b*). The crystals grew to average dimensions of 0.3 × 0.2 × 0.2 mm in ∼10 d.

Intensity data were collected on a MAR345 imaging plate installed on a Rigaku UltraX-18 rotating-anode X-ray generator operated at 50 kV and 60 mA. Individual 3° oscillation frames were collected from a single crystal at room temperature. Although the crystals diffracted to a modest resolution of 3.5 Å, the imaging plate was kept at a sufficiently large distance of 180 mm to avoid overlap of diffraction spots. The entire diffraction data were integrated and scaled using *DENZO* and *SCALEPACK* (Otwinowski & Minor, 1997). The (00*l*) reflections failed to assign the crystals to either space group $C222$ or $C222_1$. The screw axis was eventually assigned through translation-function searches. The correlation coefficient and R factor for the $C222_1$ space group were 0.621 and 0.471, respectively. The translation solution obtained in the correct $C222_1$ space group showed no intermolecular overlaps on inspection of the graphics. The data-collection statistics are given in Table 1.

2.2. Structure solution

The molecular symmetry of Mt-cpn10 was identified through a self-rotation function calculated using data in the range 12–4.5 Å with a radius of integration in the Patterson

function of 40 Å using the *POLARRFN* program (Collaborative Computational Project, Number 4, 1994) (Fig. 1). The structure was solved by molecular replacement using the main-chain coordinates of *M. leprae* chaperonin-10 heptamer (PDB code 1lep; Mande *et al.*, 1996) as a model using the *AMoRe* package as available from the *CCP*4 suite (Collaborative Computational Project, Number 4, 1994). All non-Gly residues were replaced by alanines in the molecular-replacement model. A small stretch of residues identified as a part of the mobile loop in *M. leprae* cpn10 was removed from the model. The temperature factors for the initial molecular-replacement model were set to 30 Å^2. Data in the range 30–3.5 Å were used for the molecular-replacement calculation.

The molecular-replacement model was initially refined as a rigid body, although there are deviations from perfect sevenfold symmetry in the *M. leprae* coordinates. Non-crystallographic restraints were used throughout the refinement. An NCS restraint weight of 150 was used in refinement cycles using *CNS* (Brunger *et al.*, 1998).

A subunit envelope for averaging was created by centering spheres of 5 Å radii around all atoms of the initial polyalanine model lacking the mobile loop or of 4 Å radii in later refined models that contained the mobile loop. The envelope was applied using the NCS operators obtained from the molecular-replacement solution and the density was averaged using *DM* before inspection. Coordinates were refined using either the *REFMAC* (Murshudov *et al.*, 1997) or *CNS* (Brunger *et al.*, 1998) programs. A randomly chosen 5% of the reflections were set aside for $R_{\rm free}$ calculations and the same set was retained when using either of the refinement programs.

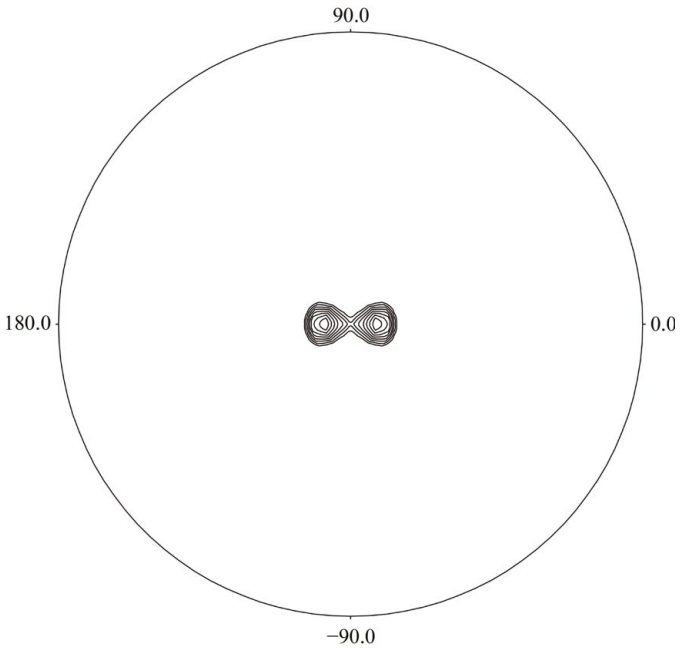

Figure 1
Plot of the self-rotation function for the Mt-cpn10 heptamer. The self-rotation function for the κ = 51.4° section was calculated using *POLARRFN* (Collaborative Computational Project, Number 4, 1994) as described in §2. The sevenfold non-crystallographic symmetry axis is present at an approximate tilt of 10° from the crystallographic *c* axis. φ angles are marked around the circumference.

A target maximum-likelihood function and the conjugate-direction method of minimization were used in *REFMAC*. All reflections to 3.5 Å were used for refinement with no low-resolution cutoff. Medium restraints for both main chains and side chains were used, but an increased weight on geometric terms was used to tighten the geometry. In addition, isotropic *B*-factor refinement by conjugate-direction minimization was also performed. Refinement cycles were interspersed with model-building sessions using the program *O* (Jones *et al.*, 1991).

The *CNS* refinement strategy used a combination of maximum-likelihood refinement of coordinates by the conjugate-gradient minimization method, group temperature factors and simulated annealing using data in the resolution range 30–3.5 Å. Group temperature factors were refined with lower and upper cutoff values of 2 and 100 Å^2, respectively, using the maximum-likelihood target function. The optimize_rweight and the optimize_wa scripts of *CNS* were used during later stages of refinement to determine the optimal values for the *B*-factor restraint weight and the geometric restraints, respectively.

Finally, a total of six iterations of *REFMAC* and nine iterations of *CNS* brought the *R* factors to acceptable levels. The refinement statistics are given in Table 1.

The final model has an acceptable geometry, with an overall *G* factor of −0.14 as reported by the *PROCHECK* program (Laskowski *et al.*, 1993). The Ramachandran plot for the heptamer shows 89.1% of the residues in the most favourable region and only one residue, Asp10, outside the allowed limits (Fig. 2). This residue has also been found outside the allowed Ramachandran limits in the *E. coli* GroES structure. Glu9 was found to occur in the Ramachandran 'generously allowed regions' in most subunits.

2.3. Search for a metal-binding site

Mt-cpn10 crystals grown as above were soaked in a solution identical to the crystallization condition except that the PEG 400 concentration was increased to 35% and $HgCl_2$ was added in incremental steps to a final concentration of 50 m*M*. The crystals were soaked in this stabilizing solution for one week before data collection. Intensity data were collected and data processing was performed as above. Finally, the native data were merged with the derivative data and scaled using the *CCP*4 program suite (Collaborative Computational Project, Number 4, 1994). These data were used to generate difference Fourier maps to identify the position of mercury binding in the crystal.

2.4. Intrinsic fluorescence measurements

Fluorimetric measurements were performed with a Perkin–Elmer LS50B luminescence spectrometer as described in Taneja & Mande (2001*a*). Briefly, the emission spectrum of 20 mg ml^{-1} Mt-cpn10 was recorded between 310 and 390 nm upon excitation at 295 nm. The scan was repeated with 5 m*M*

mercury or calcium as above. Appropriate buffer baselines were subtracted in each case. Each spectrum was an average of five scans.

2.5. Structural comparisons

The cpn10 structures were superposed using the *LSQKAB* program from the *CCP*4 suite (Collaborative Computational Project, Number 4, 1994) and visualized using *O* (Jones *et al.*, 1991). The structures used for comparison were *M. leprae* cpn10 (PDB code 1lep; Mande *et al.*, 1996), *E. coli* GroES from the GroES–GroEL complex (1aon; Xu *et al.*, 1997) and the *E. coli* mobile loop NMR structure (1egs; Landry *et al.*, 1996).

3. Results

3.1. Overall structural features

As anticipated, the overall structure of the individual Mt-cpn10 subunits conforms to the small β-barrel family known as the GroES-fold (Murzin, 1996; Taneja & Mande, 1999). The current model lacks the first four and the last two residues of each monomer, as no electron density was visible for these residues. This model therefore includes a total of 574 residues, starting with the fifth residue and ranging to the 97th residue in each monomer. There is a main-chain break at the 16th residue, where electron density for the following five residues has not been observed. Similarly, electron density for six residues joining the end of the mobile loop to the rest of the protein is not present. Nine residues of the mobile loop are clearly visible in all the seven subunits of Mt-cpn10 (Taneja & Mande, 2001*b*).

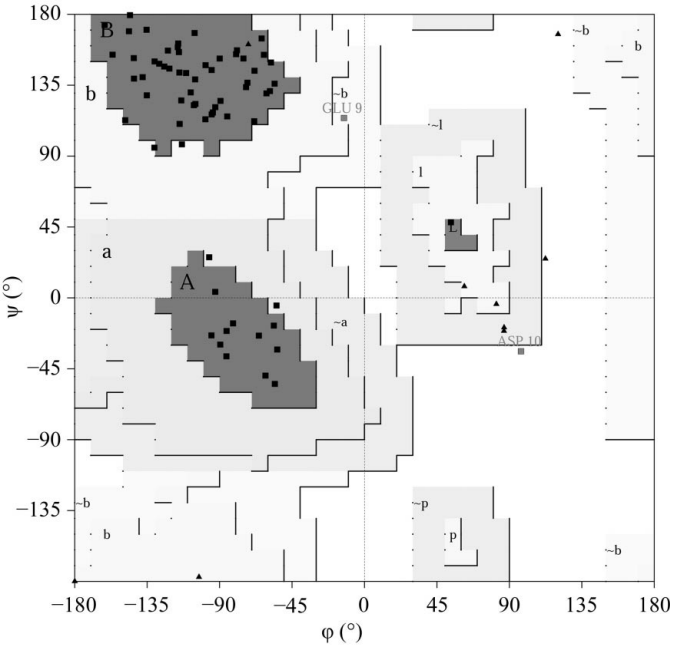

Figure 2
Ramachandran plot for one of the subunits of Mt-cpn10. The plot indicates most of the residues to be in the allowed regions. Only Asp10 was found to occur in Ramachandran disallowed regions and Glu9 in generously allowed regions (see text for details).

3.2. Conformation of the dome loop

A flexible segment of approximately ten residues (residues 49–59 in Mt-cpn10) which encloses the dome-like structure of chaperonin-10 is called as the 'dome loop' (Hunt *et al.*, 1996; Mande *et al.*, 1996; Taneja & Mande, 1999). This loop, which is also the closest approach point of the individual subunits to their sevenfold molecular symmetry axis, has been an enigmatic feature of the cpn10 structures. In a large majority of the cpn10 sequences, at least one of the three residues at the tip of this loop is acidic. The conglomeration of acidic residues appears to give an intense negative charge at the top of the dome, making the dome loop particularly unstable and dynamic (Taneja & Mande, 2001*a*). In the Mt-cpn10 structure, the three residues at the tip of the loop are Asp, Glu and Asp. Our earlier demonstration that the negatively charged loop might play an important role in chelating divalent cations and the subsequent addition of divalent metals to crystallizing solutions had made us anticipate the density of the entire loop clearly (Taneja & Mande, 2001*a*). However, side-chain density for Asp51 and Asp53 is not seen in any of the subunits.

3.3. Metal ions bind to the dome loop

Determination of the metal-binding site in Mt-cpn10 was carried out with the help of heavy metals, as calcium ions could not be unambiguously identified in the electron-density maps at the low resolution of 3.5 Å. The tryptophan fluorescence of Mt-cpn10 in the presence of mercury resulted in a blue shift in the emission maxima, indicating the burial of tryptophan in a more apolar environment. A similar effect on the intrinsic tryptophan (Trp) fluorescence of Mt-cpn10 was previously observed on addition of various metal ions, including calcium (Taneja & Mande, 2001*a*), confirming the binding of mercury to cpn10 (Fig. 3*a*). Moreover, mercury was also used for derivatization of *M. leprae* cpn10 during its structure solution (Mande *et al.*, 1996). Cpn10 crystals were soaked in an artificial mother liquor solution along with mercuric chloride to identify the preferential binding sites of metals. The mercury-derivatized crystals diffracted to a low resolution (6 Å). The merging statistics of the mercury-derivatized crystal data with that of the native data are indicated in Table 1. Difference Fourier maps resulted in unambiguous electron densities indicating a single preferential binding site for mercury in each subunit. Trp50 seems to be directly involved in mercury binding through its indole nitrogen. A similar binding site for mercury was also observed previously for the *M. leprae* cpn10 structure (Mande *et al.*, 1996). The other residues that appear to be involved in binding mercury are Glu9 of the same subunit and Asp61 of a neighbouring subunit at the base of the dome loop (Fig. 3*b*). Metal ions might therefore bind to the Trp and its neighbouring residues, resulting in decreased flexibility of the dome loop.

3.4. Structural comparisons with *E. coli* GroES and *M. leprae* cpn10

It is of interest to compare the Mt-cpn10 structure with *E. coli* GroES and *M. leprae* cpn10. The *E. coli* GroES structure available in the PDB (1aon) is in a complex with GroEL, while the *M. leprae* structure (1lep) is in an uncomplexed form. Least-squares superposition with *E. coli* GroES resulted in an r.m.s. deviation of 1.2 Å for 69 structurally equivalent residues. Similarly, superposition with *M. leprae* cpn10 resulted in an r.m.s. deviation of 0.8 Å for 73 residues. *M. tuberculosis* cpn10 shares 44 and 90% sequence identity with *E. coli* GroES and *M. leprae* cpn10, respectively. The r.m.s. deviation values obtained by least-square superpositions are therefore comparable to those observed for similarly diverged protein pairs (Chothia & Lesk, 1986). The comparison of Mt-cpn10 with that from *M. leprae* indicates deviations at regions 43–46 and 88–92. These deviations are likely to have arisen owing to differences in crystal packing.

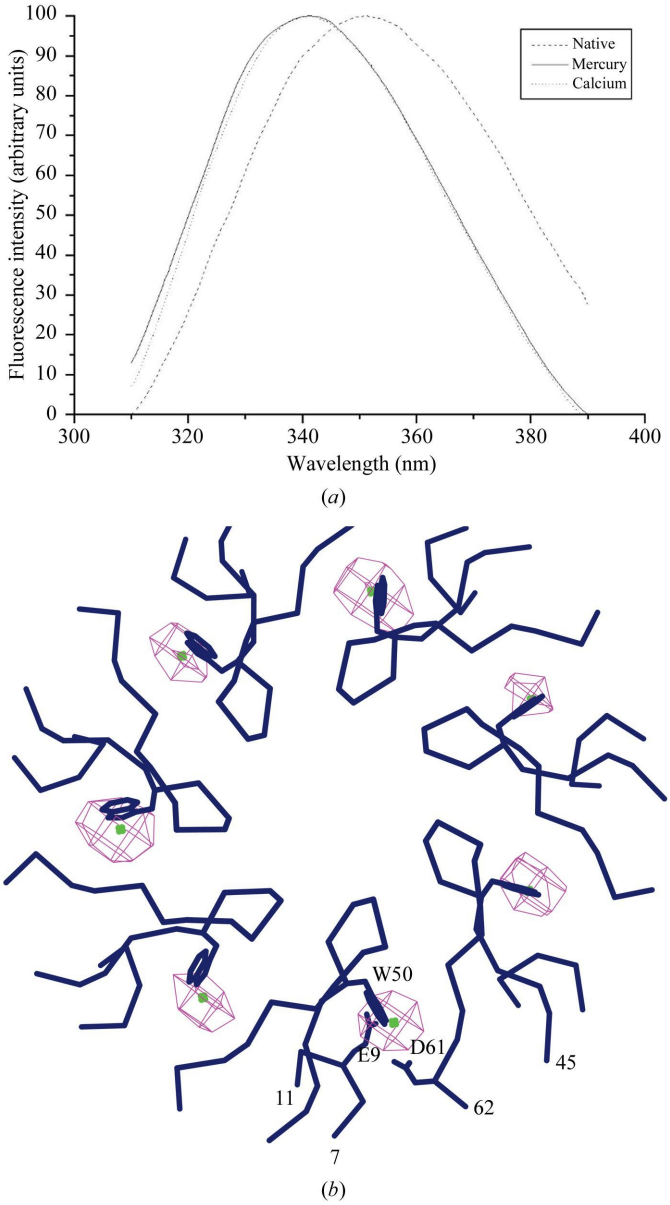

Figure 3
(*a*) Normalized emission spectra indicating the blue shift in the presence of mercury (solid line). The emission spectra of Mt-cpn10 in the absence of any metal ions (dashed line) or in the presence of calcium ions (dotted line) are indicated as controls. Thus, mercury has a similar effect on the fluorescence spectrum of the protein as other divalent cations (Taneja & Mande, 2001*a*). (*b*) Difference Fourier maps indicating the binding of mercury to the dome loop as viewed down the sevenfold axis of the heptamer. Electron-density maps contoured at three standard deviations above the mean value indicate the binding of mercury close to Trp50. The other residues in the proximity of the binding site, Glu9 of one subunit and Asp61 of another subunit, are indicated. Residues 45 and 62 at the dome and residues 7 and 11 of the neighbouring subunit are also labelled.

Comparison of the *E. coli* cpn10 structure with that of *M. tuberculosis* shows large deviations in the dome loop as well as the residues at the termini. These deviations in the dome loop can be attributed to the high flexibility of the dome loop as well as the insertion of a residue in the dome loop of the mycobacterial sequences.

In addition to these regions, comparison of the *E. coli* GroES and Mt-cpn10 structures indicates differences in another region, the 76–87 stretch. The conformational changes in Mt-cpn10 in this region have previously been shown to be important for the stabilization of the mobile-loop structure (Taneja & Mande, 2001*b*). A rigid-body movement of the entire 76–87 stretch exposes a hydrophobic patch of residues. The exposed hydrophobic patch then facilitates docking of the mobile loop of a neighbouring subunit onto the main body of the protein through interactions with a conserved hydrophobic tripeptide, LVI, of the mobile loop. The *E. coli* structure used for comparison with Mt-cpn10 is complexed with GroEL. The mobile loop in the *E. coli* GroES structure extends away from the main protein body in order to dock itself onto the GroEL chaperonin (Xu *et al.*, 1997). The conformational differences between the *E. coli* GroES and Mt-cpn10 in this region can therefore be attributed to the complex formation between GroEL and GroES (Taneja & Mande, 2001*b*).

4. Discussion

The 99-residue cpn10 is known to contain two long stretches of extremely flexible segments: one in the dome loop and one in the mobile loop (Hunt *et al.*, 1996; Mande *et al.*, 1996; Landry *et al.*, 1993). Moreover, the heptameric assembly of cpn10s is also highly plastic in solution (Timchenko *et al.*, 2000). Owing to these factors and possibly other molecular features, Mt-cpn10 is known to exist in a dynamic equilibrium between the tetrameric and heptameric states (Fossati *et al.*, 1995). We recently showed that divalent cations lead to substantial conformational changes in the molecule, particularly in the dome loop, thereby conferring stability on the heptameric assembly of the molecule (Taneja & Mande, 2001*a*). Both GroEL and GroES undergo major structural transitions during complex formation. One of the intriguing aspects of these conformational transitions is the tremendous loss in flexibility of the GroES mobile loop yet the strong GroEL–GroES association is maintained. The entropic costs of loop immobilization, estimated to be around 33 kJ mol^{-1}, must

therefore be compensated by strong enthalpic contributions from the interactions (Landry *et al.*, 1996). The Mt-cpn10 structure indicates that while the flexible dome loop of Mt-cpn10 is partially stabilized by the binding of metal ions, the highly flexible mobile loop may also overcome the high entropic cost by possessing a partially stable conformation (Taneja & Mande, 2001*b*).

Cpn10 has previously been postulated to be a major factor responsible for bone resorption in Pott's disease (Meghji *et al.*, 1997). The structure–activity relationships of Mt-cpn10 with the help of overlapping synthetic peptides have identified the mobile-loop region of Mt-cpn10 and a loop region comprising residues 65–70 to play important roles in bone resorption. The osteolytic activity of cpn10 was shown to be present in these regions, which were suggested to comprise a single conformational unit (Meghji *et al.*, 1997). This hypothesis appears to be in agreement with the Mt-cpn10 crystal structure presented in this report. Unlike the currently available crystal structures of cpn10 from *E. coli*, the mobile loop appears to be present as a single conformational unit with the residues 65–70 in Mt-cpn10. It is therefore possible that these two regions of the secreted antigen possess osteolytic activity, as proposed previously (Meghji *et al.*, 1997).

Divalent cations have previously been shown to stabilize Mt-cpn10 and decrease its oligomeric plasticity (Taneja & Mande, 2001*a*). One interesting possibility for the bone-resorbing activity of Mt-cpn10 could be that it is a consequence of the chelation of calcium ions by the chaperonin, thereby disturbing the equilibrium of calcium ions available for bone calcification. It is well known now that cpn10 of *M. tuberculosis* (Abou-Zeid *et al.*, 1988), as well as chaperones from many other microorganisms, are either actively secreted or expressed on their surface (Ranford *et al.*, 2000). This secreted Mt-cpn10 is therefore available for the chelation of calcium at bone joints. The overall depletion of calcium ions from the bone matrix might therefore lead to severe deformities in the bone.

The cpn10 from *M. tuberculosis* as well as that from *M. leprae* produces a strong immune response in tuberculosis or leprosy (Mehra *et al.*, 1992). Mt-cpn10 has previously been identified to be a major T-cell antigen during infection (Young & Garbe, 1991). Previous studies have identified specific immunodominant epitopes of the GroES homologues from *M. tuberculosis* and *M. leprae* (Kim *et al.*, 1997; Chua-Intra *et al.*, 1998). These studies using truncated overlapping peptides of the entire GroES protein mapped the strongly immunodominant epitopes to the region of the mobile loop. However, despite more than 90% sequence identity, the two antigens showed significant differences in certain epitopes derived from the two cpn10s. In particular, while the peptides spanning residues 28–39 of *M. leprae* elicited a strong immune response, homologous *M. tuberculosis* peptides from this region did not. It is interesting to note that five of the nine residues differing in the two antigens are present in the mobile-loop region 17–32. However, synthetic peptides differing in only one residue at position 31 of this peptide led to large differences in epitope affinities for MHC molecules (Chua-Intra *et al.*, 1998). These differences may be a result of specific processing or post-translational modifications of the cpn10 peptides (Rosenkrands *et al.*, 1999). It has recently been shown that the kinetics of interaction of TCR with the peptide–MHC complex are directly related to the T-cell response (Kalergis *et al.*, 2001). Point mutations that led to either shortened or prolonged half-lives of interaction were both detrimental to T-cell activation. It is hence possible that difference in a single residue of the immunodominant epitope of *M. leprae* and *M. tuberculosis* results in differing T-cell responses owing to the different kinetics of binding. Mt-cpn10 has also been successfully used to confer protective immune response against the foot-and-mouth disease virus (Amadori *et al.*, 1999). This property of Mt-cpn10 assumes immediate relevance in view of the recent spread of this disease worldwide. Although the structure does not distinctly throw light on the intricate details of these mechanisms, it lays the groundwork for further biochemical studies to understand the molecular details of the various biological roles of this important antigen.

We thank Vijay Mehra and Barry Bloom for the generous gift of *M. tuberculosis* chaperonin-10 clones. We also thank Sharmila Mande for stimulating discussions and C. M. Gupta, A. Ghosh and Wim Hol for encouragement. Financial support for the work provided by Council of Scientific and Industrial Research (CSIR) and the Department of Biotechnology, New Delhi is gratefully acknowledged. BT is a CSIR senior research fellow.

References

Abou-Zeid, C., Smith, I., Grange, J. M., Ratliff, T. L., Steele, J. & Rook, G. A. (1988). *J. Gen. Microbiol.* **134**, 531–538.
Amadori, M., Archetti, I. L., Scaccaglia, P., Modena, D., Fossati, G., Lucietto, P. & Mascagni, P. (1999). *Arch. Virol.* **144**, 905–919.
Brunger, A. T., Adams, P. D., Clore, G. M., DeLano, W. L., Gros, P., Grosse-Kunstleve, R. W., Jiang, J. S., Kuszewski, J., Nilges, M., Pannu, N. S., Read, R. J., Rice, L. M., Simonson, T. & Warren, G. L. (1998). *Acta Cryst.* D**54**, 905–921.
Chothia, C. & Lesk, A. M. (1986). *EMBO J.* **5**, 823–826.
Chua-Intra, B., Peerapakorn, S., Davey, N., Jurcevic, S., Busson, M., Vordermeier, H. M., Pirayavaraporn, C. & Ivanyi, J. (1998). *Infect. Immun.* **66**, 4903–4909.
Cole, S. T., Brosch, R., Parkhill, J., Garnier, T., Churcher, C., Harris, D., Gordon, S. V., Eiglmeier, K., Gas, S., Barry, C. E. III, Tekaia, F., Badcock, K., Basham, D., Brown, D., Chillingworth, T., Connor, R., Davies, R., Devlin, K., Feltwell, T., Gentles, S., Hamlin, N., Holroyd, S., Hornsby, T., Jagels, K., Krogh, A., McLean, J., Moule, S., Murphy, L., Oliver, K., Osborne, J., Quail, M. A., Rajandream, M.-A., Rogers, J., Rutter, S., Seeger, K., Skelton, J., Squares, S., Squares, R., Sulston, J. E., Taylor, K., Whitehead, S. & Barrell, B. G. (1998). *Nature (London)*, **393**, 537–544.
Collaborative Computational Project, Number 4 (1994). *Acta Cryst.* D**50**, 760–763.
Fayet, O., Ziegelhoffer, T. & Georgopoulos, C. (1989). *J. Bacteriol.* **171**, 1379–1385.
Fenton, W. A. & Horwich, A. L. (1997). *Protein Sci.* **6**, 743–760.
Fossati, G., Lucietto, P., Giuliani, P., Coates, A. R., Harding, S., Colfen, H., Legname, G., Chan, E., Zaliani, A. & Mascagni, P. (1995). *J. Biol. Chem.* **270**, 26159–26167.
Hartl, F. U. (1996). *Nature (London)*, **381**, 571–580.

Houry, W. A, Frishman, D., Eckerskorn, C., Lottspeich, F. & Hartl, F. U. (1999). *Nature (London)*, 402, 147–154.
Hunt, J. F., van der Vies, S. M., Henry, L. & Deisenhofer, J. (1997). *Cell*, **90**, 361–371.
Hunt, J. F., Weaver, A. J., Landry, S. J., Gierasch, L. & Deisenhofer, J. (1996). *Nature (London)*, **379**, 37–45.
Jones, T. A., Zou, J. Y., Cowan, S. W. & Kjeldgaard, M. (1991). *Acta Cryst.* A**47**, 110–119.
Kalergis, A. M., Boucheron, N., Doucey, M.-A., Palmieri, E., Goyarts, E. C., Vegh, Z., Luescher, I. F. & Nathenson, S. G. (2001). *Nature Immunol.* **2**, 229–234.
Kim, J., Sette, A., Rodda, S., Southwood, S., Sieling, P. A., Mehra, V., Ohmen, J. D., Oliveros, J., Appella, E., Higashimoto, Y., Rea, T. H., Bloom, B. R. & Modlin, R. (1997). *J. Immunol.* **159**, 335–343.
Landry, S. J., Ryalls, J. Z., Fayet, O., Georgopoulos, C. & Gierasch, L. M. (1993). *Nature (London)*, 364, 255–258.
Landry, S. J., Taher, A., Georgopoulos, C. & van der Vies, S. M. (1996). *Proc. Natl Acad. Sci. USA*, **93**, 11622–11627.
Laskowski, R. A., MacArthur, M. W., Moss, D. S. & Thornton, J. (1993). *J. Appl. Cryst.* **26**, 283–291.
Mande, S. C., Mehra, V., Bloom, B. R. & Hol, W. G. J. (1996). *Science*, **271**, 203–207.
Meghji, S., White, P. A., Nair, S. P., Reddi, K., Heron, K., Henderson, B., Zaliani, A., Fossati, G., Mascagni, P., Hunt, J. F., Roberts, M. M. & Coates, A. R. M. (1997). *J. Exp. Med.* **186**, 1241–1246.
Mehra, V., Bloom, B. R., Bajardi, A. C., Grisso, C. L., Sieling, P. A., Alland, D., Convit, J., Fan, X., Hunter, S. W., Brennan, P. J., Rea, T. H. & Modlin, R. L. (1992). *J. Exp. Med.* **175**, 275–284.
Murshudov, G. N., Vagin, A. A. & Dodson, E. J. (1997). *Acta Cryst.* D**53**, 240–255.
Murzin, A. (1996). *Curr. Opin. Struct. Biol.* **6**, 386–394.
Otwinowski, Z. & Minor, W. (1997). *Methods Enzymol.* **276**, 307–326.
Ranford, J. C., Coates, A. R. M. & Henderson, B. (2000). *Exp. Rev. Mol. Med.* 15 September, 1–17. http://www-ermm.cbcu.cm.ac.uk/00002015h.htm.
Richardson, A., Schwager, F., Landry, S. J. & Georgopoulos, C. (2001). *J. Biol. Chem.* **276**, 4981–4987.
Rosenkrands, I., Weldingh, K., Ravn, P., Brandt, L., Hojrup, P., Rasmussen, P. B., Coates, A. R., Singh, M., Mascagni, P. & Andersen, P. (1999). *Infect. Immun.* **67**, 5552–5558.
Rye, H. S., Burston, S. G., Fenton, W. A., Beecham, J. M., Xu, Z., Sigler, P. B. & Horwich, A. L. (1997). *Nature (London)*, **388**, 792–798.
Sigler, P. B., Xu, Z., Rye, H. S., Burston, S. G., Fenton, W. A. & Horwich, A. L. (1998). *Annu. Rev. Biochem.* **67**, 581–608.
Taneja, B. & Mande, S. C. (1999). *Protein Eng.* **12**, 815–818.
Taneja, B. & Mande, S. C. (2001*a*). *Protein Eng.* **14**, 391–395.
Taneja, B. & Mande, S. C. (2001*b*). *Curr. Sci.* **81**, 87–91.
Timchenko, A. A., Melnik, B. S., Kihara, H., Kimura, K. & Semisotnov, G. V. (2000). *FEBS Lett.* **471**, 211–214.
Xu, Z., Horwich, A. L. & Sigler, P. B. (1997). *Nature (London)*, **388**, 741–750.
Young, D. B. & Garbe, T. R. (1991). *Infect. Immun.* **59**, 3086–3093.